


RESEARCH ARTICLE

Integrin $\beta 3$ regulates apical dendritic morphology of pyramidal neurons throughout hippocampal CA3

Christopher J. Handwerk | Collin J. Denzler | Anna R. Kalinowski |
Hollyn N. Cook | Hilda V. Rodriguez | Katherine M. Bland | Cooper A. Brett |
Brian D. Swinehart | Elizabeth C. Vinson | George S. Vidal 

Department of Biology, James Madison University, MSC 7801, Harrisonburg, Virginia 22807, USA

Correspondence

George S. Vidal, Department of Biology, James Madison University MSC 7801, Harrisonburg, VA 22807, USA.

Email: vidalgx@jmu.edu

Funding information

National Institute of Neurological Disorders and Stroke, Grant/Award Number: K01NS107723

Abstract

In excitatory hippocampal pyramidal neurons, integrin $\beta 3$ is critical for synaptic maturation and plasticity in vitro. *Itgb3* is a potential autism susceptibility gene that regulates dendritic morphology in the cerebral cortex in a cell-specific manner. However, it is unknown what role *Itgb3* could have in regulating hippocampal pyramidal dendritic morphology in vivo, a key feature that is aberrant in many forms of autism and intellectual disability. We found that *Itgb3* mRNA is expressed in the *stratum pyramidale* of CA3. We examined the apical dendritic morphology of CA3 hippocampal pyramidal neurons in conditional *Itgb3* knockouts and controls, utilizing the *Thy1-GFP-M* line. We fully reconstructed the apical dendrite of each neuron and determined each neuron's precise location along the dorsoventral, proximodistal, and radial axes of the *stratum pyramidale*. We found a very strong effect for *Itgb3* expression on CA3 apical dendritic morphology: neurons from conditional *Itgb3* knockouts had longer and thinner apical dendrites than controls, particularly in higher branch orders. We also assessed potential relationships between pairs of topographic or morphological variables, finding that most variable pairs were free from any linear relationships to each other. We also found that some neurons from controls, but not conditional *Itgb3* knockouts, had a graded pattern of overall diameter along the dorsoventral and proximodistal axes of the *stratum pyramidale* of CA3. Taken together, *Itgb3* is essential for constructing normal dendritic morphology in pyramidal neurons throughout CA3.

KEYWORDS

autism, CA3, dendrites, dendritic morphology, *Itgb3*, pyramidal neuron

Collin J. Denzler and Anna R. Kalinowski should be considered joint second authors.

This is an open access article under the terms of the [Creative Commons Attribution-NonCommercial-NoDerivs](https://creativecommons.org/licenses/by-nc-nd/4.0/) License, which permits use and distribution in any medium, provided the original work is properly cited, the use is non-commercial and no modifications or adaptations are made.

© 2023 The Authors. *Hippocampus* published by Wiley Periodicals LLC.

1 | INTRODUCTION

Integrin $\beta 3$ is a subunit required for normal hippocampal function, and it is expressed in the developing and adult hippocampus (Chan et al., 2003; Kang et al., 2008), where it is thought to bind exclusively with integrin αV to create a functional integrin receptor (Jaudon et al., 2021; Lilja & Ivaska, 2018; Park & Goda, 2016). *Itgb3* gene mutations have been associated in particular with autism spectrum disorder, as well as with depression and schizophrenia (reviewed comprehensively by Jaudon et al., 2021).

Integrin $\beta 3$ is expressed at synapses of dissociated primary hippocampal neurons, preferentially postsynaptically (Chavis & Westbrook, 2001; Cingolani et al., 2008; Shi & Ethell, 2006), where it can bind to GluA2 (Poza et al., 2012) and is involved in GluA2 endocytic regulation at synapses (Cingolani et al., 2008). Some hippocampal functions of integrin $\beta 3$ have been elucidated through *in vitro* cell culture experiments. For example, in cultured dissociated primary hippocampal neurons, integrin $\beta 3$ is critical for a developmental switch in the probability of release (Chavis & Westbrook, 2001). Cultured hippocampal neurons also show an increase in mEPSC amplitude after exogenous expression of integrin $\beta 3$ (Poza et al., 2012) and a decrease in mEPSC amplitude after application of cilengitide, which disrupts integrin $\beta 3$ and $\beta 5$ -mediated interactions with the extracellular matrix (McGeachie et al., 2012), or echistatin, which targets integrins $\beta 3$ and $\beta 1$ (Cingolani et al., 2008). In both organotypic and dissociated hippocampal cultures, integrin $\beta 3$ is essential for synaptic scaling, a form of homeostatic plasticity (Cingolani et al., 2008; Cingolani & Goda, 2008), but is not required for short-term or Hebbian plasticity (McGeachie et al., 2012). Taken together, integrin $\beta 3$ has several crucial roles in hippocampal synaptic plasticity and maturation, at least *in vitro*.

In vivo, global *Itgb3* knockout leads to reductions in hippocampal volume (Ellegood et al., 2012), abnormal self-grooming and social behavior (Carter et al., 2011), abnormal responses to chronic unpredictable stressors (Varney et al., 2015), and abnormal anxiety-like behavior (McGeachie et al., 2012) that can be reversed by exogenous restoration of *Itgb3* expression to the ventral hippocampi (McGeachie et al., 2012). More recently, targeted deletion of *Itgb3* chiefly from neurons and astrocytes of the hippocampus and cerebral cortex caused abnormal self-grooming and sociability behaviors (Lopuch et al., 2022).

Despite these functional, behavioral and whole-brain anatomical data, very little is known about how integrin $\beta 3$ might be involved in the stability and development of neuronal morphology in the hippocampus, where other autism models have shown an effect (Barón-Mendoza et al., 2019; Cloarec et al., 2019). It is known that in dissociated hippocampal cultures, integrin $\beta 3$ regulates dendritic spine elongation mediated by RGD peptide application (Shi & Ethell, 2006) and is required for neurite retraction (Herrera-Molina et al., 2012). In proliferative Neuro2a neuroblastoma cultures, *Itgb3* deletion increases the number of cells with complex dendritic arborizations and increases total neurite length (Riccardi et al., 2022). Finally, *in vivo* evidence from the cerebral cortex shows that *Itgb3* deletion in layer 2/3 cortical pyramidal neurons cell-specifically increases dendritic length by

postnatal day 23 (Swinehart et al., 2020). It is entirely unknown, however, whether integrin $\beta 3$ is required for shaping the overall dendritic morphology of hippocampal pyramidal neurons *in vivo*.

To answer this question, we assessed the *in situ* expression of *Itgb3* in the hippocampus and found it to be expressed mostly in the *stratum pyramidale* of CA3. We also compared the apical dendritic morphology of *Thy1*-GFP-M-labeled CA3 hippocampal pyramidal neurons in conditional knockouts (“cKO” where *Itgb3* is deleted from chiefly hippocampal and cortical excitatory neurons and astrocytes) to *Thy1*-GFP-M-labeled CA3 hippocampal pyramidal neurons in controls. Knowing that there may be considerable morphological variation along the dorsoventral, proximodistal, and radial axes of the hippocampus (Handwerk et al., 2022; Hunt et al., 2018; Sun et al., 2020), we also controlled for the precise cellular position of each CA3 neuron we analyzed. We also controlled for potential clustering of data collected from multiple hippocampi. Results show a strong effect of *Itgb3* expression on the apical dendritic morphology of CA3 hippocampal pyramidal neurons.

2 | METHODS

2.1 | Ethics statement and data availability

This study, which necessitated work with mice, was approved by the James Madison University Institutional Animal Care and Use Committee (protocol #20-1067), and the Guide for the Care and Use of Laboratory Animals was followed. The reconstruction data that support the findings of this study will be made openly available at NeuroMorpho.org (Akram et al., 2018; Ascoli et al., 2007). Other data are available from the corresponding author upon reasonable request.

2.2 | Mice

For this study, we generated control mice with transgenic green fluorescent protein (GFP) labeling (hereafter called “WT” because they are the group closest to “wild type”) and *Itgb3* conditional knockout mice with transgenic GFP labeling (“cKO”). To do so, we initially acquired the following four mouse lines from The Jackson Laboratory: C57BL6/J mice (The Jackson Laboratory Cat# 000664 RRID:IMSR_JAX:000664), *Thy1*-GFP-M mice (G. Feng et al., 2000) (STOCK Tg(Thy1-EGFP)MJrs/J, The Jackson Laboratory Cat# 007788, RRID:IMSR_JAX:007788), floxed *Itgb3* mice (Morgan et al., 2010) (C57BL/6-*Itgb3*^{tm1.1VWbcr}/J, The Jackson Laboratory Cat# JAX_028232, RRID:IMSR_JAX:028232), and *Emx1*-Cre mice (Gorski et al., 2002) (B6.129S2-*Emx1*^{tm1(cre)}Krj/J, The Jackson Laboratory Cat# 005628, RRID:IMSR_JAX:005628). The *Thy1*-GFP-M mice, which are always kept as hemizygotes in our colony, had been bred for at least five generations to C57BL6/J mice, using only males to pass on the *Thy1*-GFP-M transgene to progeny, prior to generating the mice for this study. We had also backcrossed floxed *Itgb3* mice at least five generations to C57BL6/J mice prior to generating the mice for this study. *Emx1*-Cre mice were already backcrossed to C57BL6/J mice for 12 generations

when we acquired them from The Jackson Laboratory. Male, *Itgb3^{fl/+}*; *Emx1^{cre}*; *Thy1-GFP-M*-positive mice or male *Thy1-GFP-M*-positive mice were crossed to female *Emx1^{cre}* mice to generate *Emx1^{cre}*; *Thy1-GFP-M*-positive mice ("WT" mice). Male *Itgb3^{fl/+}*; *Emx1^{cre}*; *Thy1-GFP-M*-positive mice and female *Itgb3^{fl/+}*; *Emx1^{cre}* mice were crossed to generate *Itgb3^{fl/fl}*; *Emx1^{cre}*; *Thy1-GFP-M*-positive mice ("cKO" mice). For this study, we collected hippocampi from two female *Emx1^{cre}*; *Thy1-GFP-M*-positive mice ("WT" mice) and three *Itgb3^{fl/fl}*; *Emx1^{cre}*; *Thy1-GFP-M*-positive mice ("cKO" mice; one female and two males). The estrous state of the young females (postnatal day 30) was not assessed. The *Emx1-Cre* line expresses Cre recombinase prenatally and strongly in targeted neurons (Gorski et al., 2002), and our prior work demonstrates a reduction of integrin $\beta 3$ expression in juvenile *Itgb3^{fl/fl}*; *Emx1^{cre}* mice (Swinehart et al., 2020). All mice used for this study were hemizygous for the *Thy1-GFP-M* transgene, and the only known difference between the two groups of mice was the presence or absence of the floxed *Itgb3* targeted mutation on both alleles. We determined the genotypes of all mice by sending ear punch tissue for genotyping (Transnetyx, probes "Thy1-3 Tg," "Itgb3-3 WT," and "Itgb3-3 KO"). Mice for this study were housed as described previously (Swinehart et al., 2020).

2.3 | *In situ* hybridization

We euthanized and perfused an adult (postnatal day 117) male WT mouse and an adult (postnatal day 117) male cKO mouse, as described previously (Swinehart et al., 2020). After 2 days of postfixation in 4% paraformaldehyde (in 1 \times PBS), we took 40- μ m coronal sections containing hippocampus proper with a VT1000S Vibratome (Leica Microsystems). Sections were incubated in 3% hydrogen peroxide (in water) for 15 min, mounted on glass slides, dried at room temperature, and frozen. We used the RNAscope Multiplex Fluorescent Manual Assay (ACD Bio), following the manufacturer's protocol, using the "Mm-Itgb3" probe (ACD Bio, cat. #481451) and Opal 570 dye (Akoya Biosciences). We mounted the sections with ProLong Diamond media (ThermoFisher) and a #1.5 glass coverslip. After the mountant had cured, we imaged the sections on a Nikon Eclipse Nikon Eclipse Ti-2 microscope with a 4 \times PlanApo objective (0.20 NA) to capture Opal 570 signal (excitation filter: 542–582 nm, emission filter: 604–678 nm), as well as DAPI signal (excitation filter: 381–403 nm, emission filter: 417–477 nm).

2.4 | Histology and microscopy for dendritic analysis

We euthanized and perfused mice at postnatal day 30, as described previously (Swinehart et al., 2020). Hippocampi were dissected and straightened along the long axis. This allowed us to make exact transverse sections of hippocampus at 100 μ m with a VT1000S Vibratome (Leica Microsystems), taking care to preserve the dorsoventral position of each section. We then immunostained the sections for GFP (to enhance GFP signal) and PCP4 (to label CA2 pyramidal neurons),

and imaged as described previously (Handwerk et al., 2022). We collected information from four WT hippocampi (two left and two right) and five cKO hippocampi (three left and two right). To determine dorsoventral topographic information, we imaged 166 total sections: 80 sections from WT (18, 16, 24, and 22 sections from WT hippocampi 1–4, respectively; some WT2 data were reported in Handwerk et al., 2022) and 86 sections from cKO (25, 12, 23, 8, and 18 sections from cKO hippocampi 1–5, respectively).

2.5 | Dendritic reconstruction and analysis

We 3D reconstructed neurons using neuTube (Feng et al., 2015) and Fiji software (Schindelin et al., 2012) with the Simple Neurite Tracer plugin (Longair et al., 2011), as described previously (Handwerk et al., 2022). To determine radial and proximodistal topographic information, and to determine morphological information, we imaged, reconstructed, and analyzed a total of 121 neurons from 62 sections (54 WT neurons from 26 WT sections and 67 cKO neurons from 36 cKO sections), creating .swc files. In WT, 11/6, 17/9, 8/4, and 18/7 neurons/sections were taken from WT hippocampi 1–4, respectively. In cKO, 15/6, 6/2, 22/13, 10/7, and 14/8 neurons/sections were taken from cKO hippocampi 1–5, respectively.

Using L-Measure software (Scorcioni et al., 2008), as described previously (Handwerk et al., 2022), we collected 10 topographic and 24 morphological variables from each reconstructed neuron. Of the 10 topographic variables, five pertain to the dorsoventral axis of the neuron (CA2 length, CA3 length, DG length, DG width, and dorsoventral position), one pertains to the radial axis (depth in *stratum pyramidale*), one controls for sectioning (depth in section), and three pertain to the transverse axis (transverse distance from CA2, transverse distance from DG, and relative transverse distance). Positive dorsoventral position values indicate more dorsal sections. Relative transverse distance values close to 1 are proximal to dentate gyrus, whereas values close to 0 are most distal from dentate gyrus. Of the 24 morphological variables, 10 pertain to the length of dendritic segments (total length, Euclidean length, path length, primary length, secondary length, tertiary length, quaternary length, quinary length, senary length, and septenary length), eight pertain to their diameter (overall diameter, primary diameter, secondary, tertiary diameter, quaternary diameter, quinary diameter, senary diameter, and septenary diameter), and six pertain to the number of branches (total branch points, tertiary branches, quaternary branches, quinary branches, senary branches, and septenary branches).

2.6 | Statistical analysis and rigor

We followed prior methods (Yu et al., 2022) to estimate the effective sample size (ESS) of analyzed neurons, which is smaller than the actual sample size due to clustering. In the context of this study, the greatest potential for clustering is for data from each of the hippocampi of one condition (e.g., the five cKO hippocampi) to differ from one another

("inter-hippocampus variability," as it were). In other words, the ESS could be in between the number of hippocampi used per condition (on one extreme, if there were complete clustering), and the number of neurons analyzed per condition (on the other extreme, if there were no clustering at all). We additionally used ANOVA (see below) to test for potential clustering between hippocampi taken from each animal. No data were excluded in analyzing the effect of clustering: Clustering reduces the ESS, but this is a calculated value, not an actual reduction in the data used.

The ESS was calculated as follows. ESS is the number of neurons analyzed in a hippocampus divided by the design effect (DE). The DE is equal to one plus the product of the interclass correlation (ICC) and one less than the average number of neurons analyzed per hippocampus. The ICC is the square of the variance among the hippocampi divided by the sum of the square of the variance among the neurons analyzed in a hippocampus and the square of the variance among the hippocampi.

We implemented two methods to reduce the chance of Type I statistical errors in our study (the false rejection of the null hypothesis). First, when comparing WT to cKO, we used nested *t* tests (GraphPad Prism 9), which considers the potential for any clustering among the data and consequent reduction in the ESS. Second, we corrected for the false discovery rate (FDR) of multiple nested *t* tests by setting an FDR threshold of 10% (Benjamini et al., 2006). In other words, the first method (ESS/nested *t* tests) ensured that we did not overestimate (or underestimate) our ESS. The second method (FDR) protected against falsely rejecting the null hypothesis due to using multiple *t* tests in our pairwise comparisons.

We also graphed QQ plots for each nested *t* test to investigate the normality of the data. We utilized multiple two-way analysis of variance (ANOVA) to investigate potential interaction effects for genotype (WT vs. KO), laterality (left vs. right hippocampus), and sex (female vs. male). Higher-order ANOVA was not possible because it cannot account for any missing values. We utilized one-way ANOVA with Tukey's multiple comparisons to investigate interanimal variability and two-way ANOVA to investigate potential interaction effects for animal and laterality. Pearson's correlations among WT or cKO topographic and/or morphological variables were run as described previously (Handwerk et al., 2022). We used GraphPad Prism 9 for all statistical analysis and graphing for all figures.

2.7 | Sholl analysis

We analyzed 3D-reconstructed WT and cKO apical dendrites with a modified version of Sholl's method (Sholl, 1953). We imported WT and cKO .swc reconstructions directly into the Sholl Analysis plugin for FIJI (Ferreira et al., 2014). We chose the center of soma as our starting point, measured radially outward in three dimensions at 10 μm increments, and only counted .swc compartments classed as apical dendrites. We then compared WT to cKO at each 10- μm distance out from the soma (to 460 μm , which is the furthest we detected an intersection in at least one WT and cKO cell). Statistical

analyses of Sholl data are prone to Type I statistical error (Wilson et al., 2017). We sought to reduce this error in our analysis, and accounted for clustering in our data (i.e., "inter-hippocampal variability") by using nested *t* tests (GraphPad Prism 9) to compare WT and cKO at each of the 46 intersections. We also set an FDR of 10% to reduce the chance of committing a Type I error by using multiple (46) nested *t* tests.

2.8 | Analysis of dorsoventral/proximodistal relationships to overall diameter

In Figure 4, we divided the data into neurons above or below the sample mean overall diameter and used a simple linear regression to test the relationship between dorsoventral position and overall diameter within each subgroup. We then subtracted an amount *t* from the dorsoventral position to account for a potential additional influence of proximodistal position on the overall diameter of the neuron. This was the product of an arbitrary scalar *u* with the absolute difference from the neuron to a fixed relative distance *v*. We found that the values of *u* and *v* that produced the best fit (as determined by simple linear regression) were *u* = 17.5 and *v* = 0.65, applied to WT neurons above the sample mean. We used these values in calculating Figure 5.

3 | RESULTS

Itgb3 mRNA was present mainly in the *stratum pyramidale* of CA3 in adult WT (but not cKO) hippocampus (Figure 1, top row). GFP labeling of pyramidal neurons was sparse throughout CA3 in both WT and cKO (Figure 1, middle row). PCP4 consistently labeled CA2, which could also be confirmed by the tapering of the GFP-labeled mossy fiber tract passing through the *stratum lucidum* of CA3 (Figure 1, middle row). GFP labeling was sparse enough to fully reconstruct apical (but not basal) dendrites, in both WT and cKO tissue (Figure 1, bottom row). For each neuron, a set of topographic (i.e., cell positioning) values and a set of morphological values were collected (e.g., Table 1).

CA3 pyramidal neurons from cKO had 35% greater total apical length than WT CA3 hippocampal pyramidal neurons (Figure 2a, Table 2). The increase in total apical dendritic length among cKO CA3 neurons could be distributed evenly across the entire apical dendrite, or it could be concentrated in a particular dendritic branch order. We found no difference between WT and cKO primary, secondary, or tertiary apical length, but did find a 49% increase in the quaternary apical length (Figure 2a, Table S1). The length from the soma to the furthest apical tip was also longer in cKO, whether it was measured as the crow flies (Euclidean length) or along the dendritic path (path length; Figure 2a, Table S1).

The total number of branch points appears to be greater in the cKO (Figure 2b), but this effect is not distinguishable from the null hypothesis. This is likely because we accounted for expected "inter-hippocampal variability," or data clustering, in our statistical methodology (Table 2). A similar pattern between WT and cKO is found in

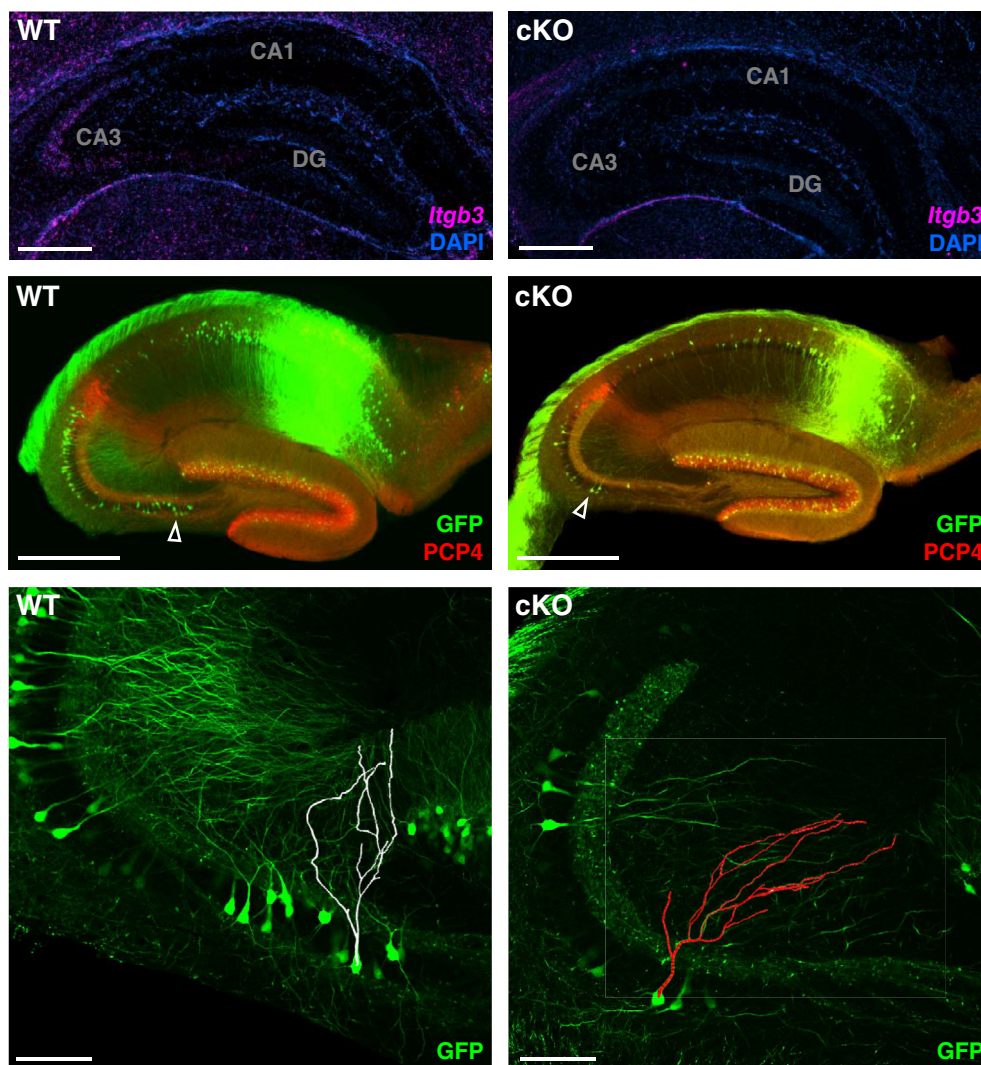


FIGURE 1 Top row: expression of *Itgb3* mRNA in *stratum pyramidale* of CA3 in a coronal section of adult WT (but not cKO) mouse hippocampus proper. Scale bars: 0.5 mm. Middle row: GFP expression and PCP4 expression in transverse sections of the WT and cKO mouse hippocampus proper. Arrowheads indicate the somata of 3D reconstructed neurons shown in the bottom row. Scale bars: 0.5 mm. Bottom row: 3D reconstructed volumes of pyramidal neuron apical dendrites in the *stratum pyramidale* of WT and cKO CA3, overlaid on a single confocal section showing GFP expression. Morphological and topographic variables for these neurons are presented in Table 1. Scale bars: 100 μ m.

TABLE 1 Morphological and topographic values for example neurons from Figure 1.

Variable	WT	cKO
Total length (μ m)	1100	1769
Euclidean length (μ m)	303	378
Path length (μ m)	358	423
Overall diameter (μ m)	2.11	1.88
Total branch points	7	10
CA2 length (μ m)	243	213
CA3 length (μ m)	938	1207
DG length (μ m)	868	952
DG width (μ m)	287	269
Dorsoventral position (μ m)	300	100
Depth in <i>s. pyramidale</i>	-28	-23
Depth in section	0.73	0.46
Transverse distance from CA2 (μ m)	907	502
Transverse distance from DG (μ m)	31	704
Relative transverse distance	0.97	0.42

higher branch orders (Figure 2b, Table S1) but again, this difference is not distinguishable from the null hypothesis (Table S1). Sholl analysis shows a similar pattern, in which the mean number of cKO intersections appears to be consistently larger than WT at distances further than 100 μ m from the soma (Figure 1a), but this difference is, yet again, not distinguishable from the null hypothesis (Figure S1b).

The overall diameter of the dendrites was smaller in cKO, when compared to WT (Figure 2c, Table 2). The reduction in overall apical dendritic diameter in the cKO could be distributed evenly across all branch orders or concentrated in a subset of them. The diameter of early branch orders (primary, secondary, and tertiary) in the cKO was not different from WT, but it was lower at all higher orders (quaternary and above) (Figure 2c, Table S1).

There exist several potential confounding factors that, if uncontrolled, could have limited our understanding of the effect of conditional *Itgb3* deletion on the morphology of CA3 hippocampal pyramidal neurons. One of them is that we could have inadvertently and preferentially selected neurons of one group (WT or cKO) from one location in the hippocampus (along the dorsoventral, proximodistal, or radial axes). This would only be a confounding factor if there

FIGURE 2 (a–c) Apical dendrites of *Itgb3* cKO CA3 hippocampal pyramidal neurons are longer and have smaller overall diameters than WT. (a') *Itgb3* cKO CA3 hippocampal pyramidal neurons have longer quaternary apical dendrites than WT. (a'') *Itgb3* cKO CA3 hippocampal pyramidal neurons are longer, measured as the crow flies from the soma to the furthest apical dendritic tip (Euclidean), or along the dendritic path. (b') Number of branches in *Itgb3* cKO CA3 hippocampal pyramidal neurons do not differ from WT. (c') *Itgb3* cKO CA3 hippocampal pyramidal neurons have smaller-diameter high order apical dendrites than WT (quaternary and above). **p*-values below the 10% FDR threshold (0.0481). All *p*-values were adjusted for potential clustering by hippocampus (see Methods and Table 2). N, mean, SEM, *p*-values, and clustering information (i.e., interclass correlation and estimated sample size) are shown in Table 2 for a–c, and in Table S1 for everything else.

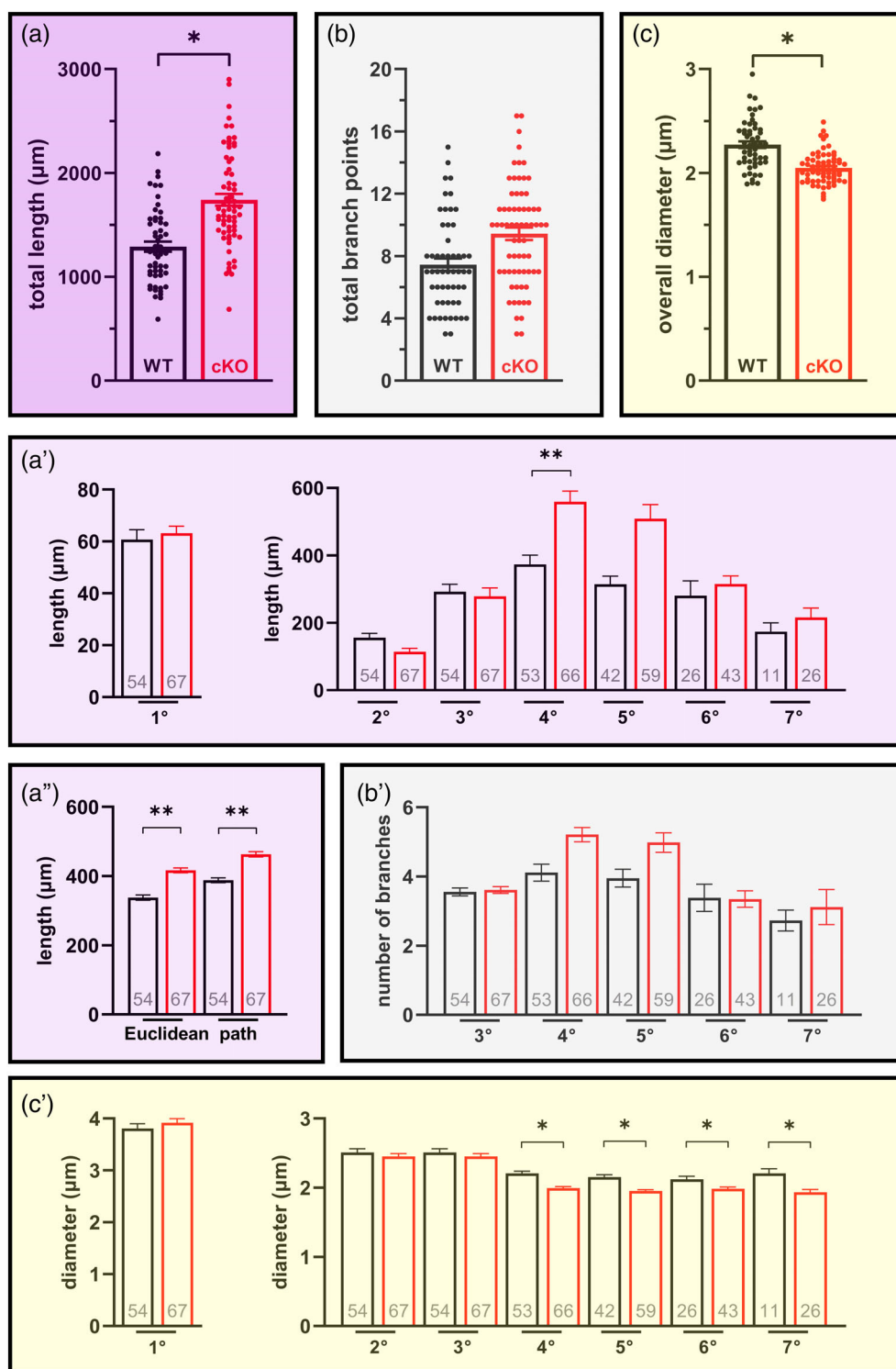


TABLE 2 Overall morphological variables (see Figure 2a–c).

Variable	WT N	WT mean	WT SEM	cKO N	cKO mean	cKO SEM	<i>p</i> -value (unadj.)	WT ICC	WT ESS	cKO ICC	cKO ESS	<i>p</i> -value (adj.)
Total length (μm)	54	1291	49	67	1741	57	<.0001	0.04	37.5	0.24	17.1	.0239
Total branch points	54	7.4	0.4	67	9.4	0.4	.0008	0.04	34.6	0.10	30.2	.0762
Overall diameter (μm)	54	2.27	0.03	67	2.05	0.02	<.0001	0.22	14.3	0.14	24.1	.0349

Note: WT N, mean, and SEM published in Handwerk et al. (2022). Bolded *p*-value is under the 10% FDR threshold ($p < .0481$). Abbreviations: ICC, interclass correlation; ESS, estimated sample size; SEM, standard error of the mean.

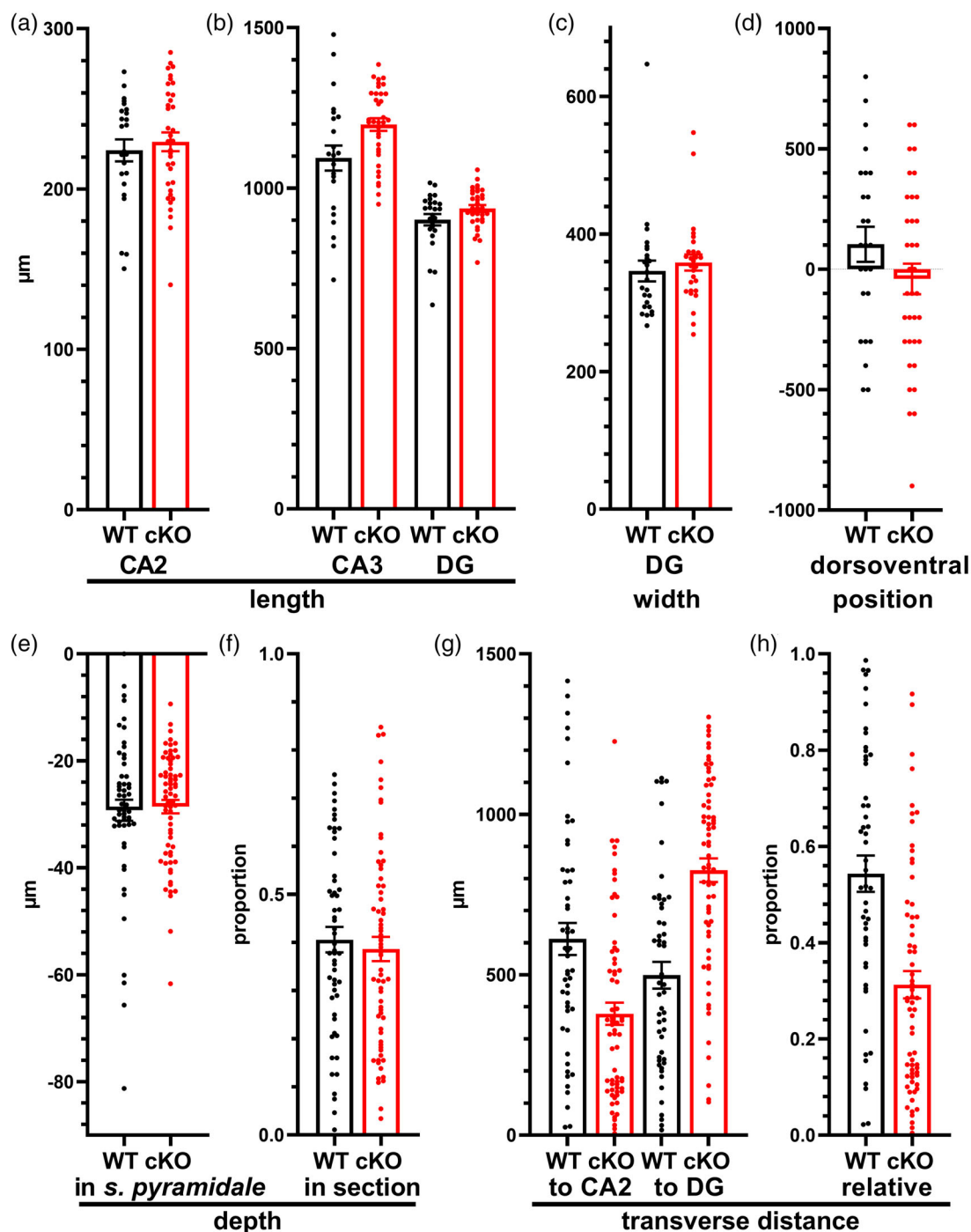


FIGURE 3 Topographic position of cKO neurons is not different from WT neurons. For dorsoventral position, positive values indicate more dorsal positions; for depth in *stratum pyramidale*, zero is the superficial border of the *stratum pyramidale*; for depth in section, “0” is the part of the section closest to the coverslip and “1” is the part of the section closest to the glass slide; and for relative transverse distance, “0” is the part of the *stratum pyramidale* closest to the border with CA2 and “1” is the part of the *stratum pyramidale* closest to dentate gyrus. Adjusted p -values are all above the 10% FDR threshold ($p < .0319$). N, mean, SEM, p -values, and clustering information (ICC and ESS) are shown in Table 3.

were also a strong effect of the location of a CA3 neuron on its morphology. We found that measurements indicating the dorsoventral position of the neuron (CA3 length, CA2 length, DG length, DG width, and dorsoventral position) were not different overall between WT or cKO (Figure 3, Table 3). Our WT or cKO neurons were also not

different along the radial axis, at a different depth in section overall, or at a different transverse position overall (Figure 3, Table 3). Another potential confounding variable is a strong effect of other factors besides genotype, such as the laterality of the hippocampus (left vs. right), the sex of the animal, or variation among individual animals.

TABLE 3 Topographic variables (see Figure 3).

Variable	WT		WT		cKO		p-value (unadj.)	WT ICC	WT ESS	cKO ICC	cKO ESS	p-value (adj.)
	N	mean	SEM	N	mean	SEM						
CA2 length (μm)	24	224	7	36	229	6	.5933	0.10	15.9	0.11	21.5	.7634
CA3 length (μm)	23	1094	39	35	1198	20	.0120	0.21	11.6	0.43	9.8	.2666
DG length (μm)	25	902	18	34	939	11	.0702	0.05	19.6	0.03	29.1	.2082
DG width (μm)	25	346	15	28	359	12	.4976	<0.01	24.7	0.04	24.0	.5201
Dorsoventral position (μm)	25	104	73	37	-57	61	.0968	0.20	12.2	0.17	17.9	.3765
Depth in <i>s. pyramidale</i>	47	-28	2	67	-29	1	.7916	0.13	19.3	0.07	37.1	.8419
Depth in section	54	0.41	0.03	67	0.39	0.03	.5998	0.04	37.4	<0.01	66.4	.6477
Transverse distance from CA2 (μm)	51	612	50	66	378	35	.0001	0.51	7.3	0.03	46.6	.1473
Transverse distance from DG (μm)	52	499	41	67	826	37	<.0001	0.41	8.8	<0.01	64.1	.0319
Relative transverse distance	50	0.54	0.04	66	0.31	0.03	<.0001	0.39	9.0	0.01	58.8	.0600

Note: WT N, mean, and SEM published in Handwerk et al. (2022). No p-values are under the 10% FDR threshold ($p < .0319$).

Abbreviations: SEM, standard error of the mean; ICC, interclass correlation; ESS, estimated sample size.

We also investigated the potential influence of other factors, such as sex and laterality (Figure S2, Table S2), or individual animal (Figure S3, Table S3). Finally, another potential confounding factor would be if the data for nested *t* tests violated the assumption of normality, but QQ plots show that the data were normal for morphological (Figure S7) and topographic data (Figure S8).

Most topographic and morphological variables were not linearly correlated to one another in WT or cKO tissue, and there were no salient differences in correlated topographic or morphological variables between WT and cKO (Figures S4 and S5). No topographic variables were linearly correlated with any morphological variables among multiple hippocampi (data not shown). These results, of course, do not exclude the possibility that there could be nonlinear relationships among the variables. For example, DG width is negatively correlated with dorsoventral position more ventrally, whereas at more dorsal positions, the two variables are positively correlated (Figure S6).

Linear correlations (Figures S4 and S5) also cannot exclude the phenomenon of Simpson's paradox, where subsets of pooled data are correlated differently than the pooled data. Thus, we investigated this possibility across pairs of topographic and morphological variables in WT and cKO neurons and found a potential relationship between dorsoventral position and overall diameter: When pooled together, neither the WT or the cKO had any positive or negative correlation between these two variables (Figure 4, top row). However, when dividing the data into above-average-diameter neurons and below-average-diameter neurons, a positive linear relationship was found in above-average-diameter WT neurons, but not in cKO neurons (Figure 4, top row).

We investigated whether variables from other topographic axes could have an additive effect on the positive linear relationship between dorsoventral position and overall diameter, so we adjusted the dorsoventral position of the neuron by a factor related to its relative transverse distance (see Methods). We found that accounting for both the dorsoventral and proximodistal position of the neuron resulted in a higher positive correlation in the above-average-diameter

WT neurons ($r^2 = 0.5056$ vs. 0.2592) (Figure 4, bottom left). Interestingly, this additive effect was not observed in the below-average-diameter WT neurons, nor in any grouping of cKO neurons (Figure 4, bottom row).

Figure 5 illustrates a model for the overall apical dendritic diameter along the dorsoventral and proximodistal axes, among above-average-diameter WT neurons. In this model, the largest diameter neurons would be expected at the most dorsal positions, with a relative transverse position of 0.65 (i.e., 65% of the way to the dentate gyrus from the border of CA2/3 along the *stratum pyramidale*). The smallest diameter neurons would be expected to be found at the most ventral positions, close to the border with either DG or CA2.

4 | DISCUSSION

We found that *Itgb3* expression is crucial for proper dendritic morphology in CA3 hippocampal pyramidal neurons. Its deletion results in longer and thinner apical dendrites. This occurs regardless of neuronal location along the proximodistal, dorsoventral, or radial axes. We found that the morphological effect of *Itgb3* deletion is localized to higher order branches.

The dendritic morphology of pyramidal neurons in cerebral cortical layer 2/3 is also regulated by *Itgb3* (Swinehart et al., 2020). In those neurons, the deletion of *Itgb3* also causes the total dendritic length to increase, similarly to our observations in CA3 neurons (overall diameter was not measured in that study). However, in the cortex, the effect of *Itgb3* deletion increases the length mainly by increasing the number of primary basal dendrites, not by increasing apical dendritic length (as occurs in CA3). Thus, it is plausible that the mechanism of action of *Itgb3* is compartmentalized differently in the two pyramidal cell populations.

Other integrin subunits are known to regulate dendritic morphology in the hippocampus (Kerrisk et al., 2013; Warren et al., 2012). Conditional deletion of either integrin $\alpha 3$ (Kerrisk et al., 2013) or $\beta 1$

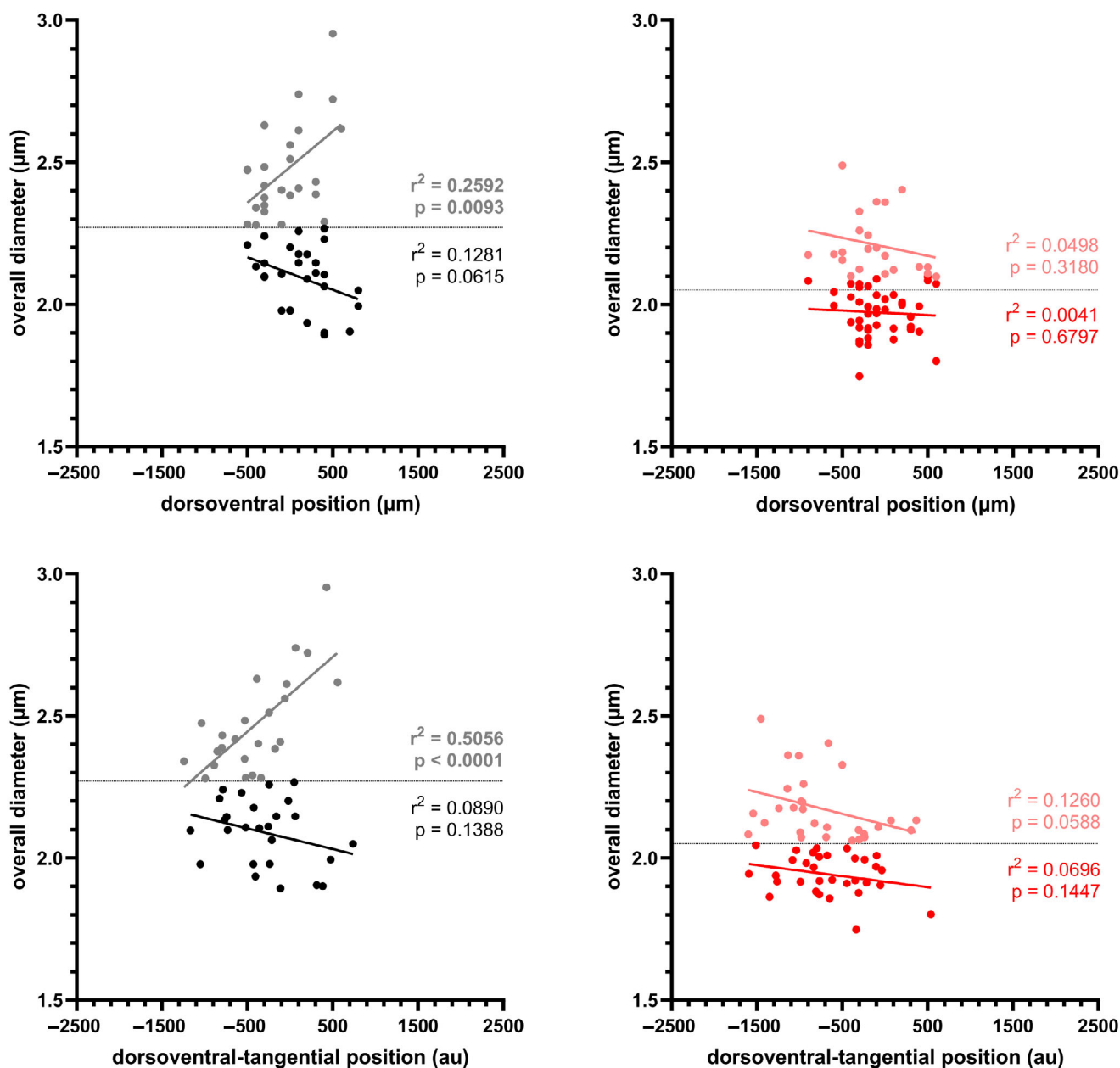


FIGURE 4 Top row: Overall diameter of apical dendrites as a function of dorsoventral position in WT (top left) and cKO (top right). Horizontal line indicates the mean overall diameter, so darker points represent below-average-diameter neurons (WT: black, cKO: red) and lighter points represent above-average-diameter neurons (WT: gray, cKO: pink). Simple linear regressions on each of the four groups are presented. Bottom row: Overall diameter of apical dendrites as a function of dorsoventral and proximodistal position, presented in the same way as the top row. New simple linear regressions on each of the four groups are presented.

(Warren et al., 2012) led to decreases of dendritic length and apical dendritic complexity at postnatal day 42 (but not at day 21). Each of these two subunits could bind to multiple other integrin subunits in the brain, but the Arg kinase pathway was involved in the actions of both integrin $\alpha 3$ and $\beta 1$, suggesting $\alpha 3\beta 1$ as the responsible heterodimer. In our case, integrin $\beta 3$ has one known partner in the brain, αV , and there is no known link between $\alpha V\beta 3$ and Arg kinase so far. Furthermore, our results show an opposite effect of integrin $\beta 3$ deletion (increased dendritic length), at a different time (postnatal day 30).

Although we cannot directly compare these studies in CA1 to ours in CA3, it is reasonable to think that integrin $\beta 3$ likely acts upon dendritic morphology through a separate molecular pathway than that of integrin $\alpha 3\beta 1$.

The function of CA3 pyramidal neurons is known to vary substantially along its dorsoventral, proximodistal, and radial axes (Cembrowski & Spruston, 2019; Hemond et al., 2009; Hemond et al., 2008; Perez-Rosello et al., 2011; Sun et al., 2017). We observed a relationship between morphology and position in some WT neurons

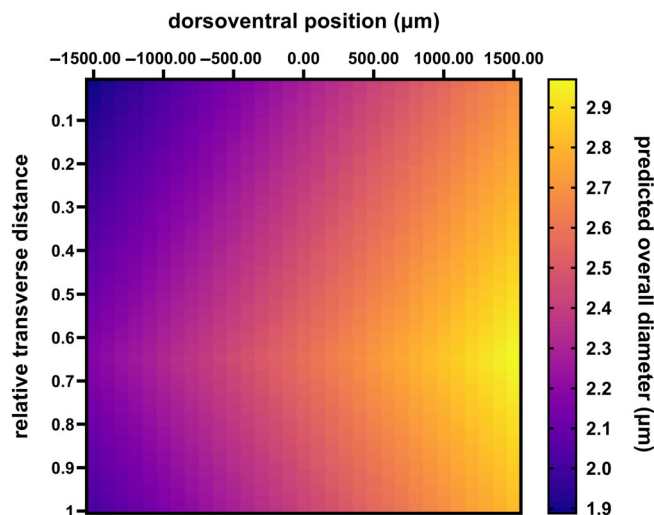


FIGURE 5 Heat map showing the predicted overall diameter of above-average-diameter WT neurons as a function of dorsoventral position and relative transverse position.

(Figures 4 and 5), adding to the body of knowledge of how CA3 pyramidal dendritic morphology relates to somatic position along these axes (Handwerk et al., 2022; Hunt et al., 2018; Ishizuka et al., 1995; Li et al., 1994; Sun et al., 2020; Turner et al., 1995). On the other hand, we did not find the somatic position of CA3 neurons to be linearly correlated with any other morphological parameter of the apical dendrites. This result is similar to Ishizuka et al. (1995), where CA3 pyramidal dendrites passing through the *stratum radiatum* (presumably the bulk of the apical dendrites we studied) did not show an overall change in dendritic length at different somatic positions. Dendrites passing through other layers, such as the *stratum oriens* (presumably basal dendrites) did show such a relationship (Ishizuka et al., 1995). A constant apical (but not basal) dendritic length is also a feature found in most of the middle of the dorsoventral axis among CA1 pyramidal neurons (Malik et al., 2016). Nonetheless, we did observe that WT did show a dorsoventral/proximodistal gradient of dendritic morphology, whereas cKO did not. This is similar to results from the cerebral cortex, where we observed a rostralateral-to-caudomedial gradient of dendritic complexity in WT but not in cKO (Swinehart et al., 2020).

Itgb3 is important for regulating the dendritic length of pyramidal neurons in both the cortex (Swinehart et al., 2020) and the hippocampus (this study), albeit differently. Compared to WT mice, cKO mice have abnormal self-grooming and sociability behaviors (Lopuch et al., 2022). Is there a link between the altered anatomy and altered behavior? The tight theoretical relationship between CA3 dendritic morphology and firing rate (Krichmar et al., 2002), as well as observed concomitant heterogeneity in both CA3 morphology and firing rate in vivo (Ding et al., 2020) suggest that there may be a link. In the case of CA3, the apical dendrites studied here—and altered by *Itgb3* deletion—mostly pass through *stratum radiatum*, the site of mostly recurrent CA3-to-CA3 (autoassociative) connections (Witter, 2007). Other pathways, such as the mossy fibers and the perforant path, mostly pass through other strata that were not analyzed (such as *stratum oriens*) or are otherwise far from the fourth apical branch

order, where we observed the most significant changes in the cKO. Because autoassociative recurrent connectivity in CA3 is required for spatial encoding, working memory, novelty detection, and cued recall (Kesner, 2007), it is plausible that the cKO would have deficits in one or more of these CA3-mediated behavioral functions.

Several limitations apply to this study. For example, our method only permitted us to assess the effect of *Itgb3* deletion on apical dendrites of CA3 pyramidal neurons, so we do not know its effect on basal dendrites of CA3, or its effect (if any) on pyramidal neurons in CA1 or CA2. We also cannot know about the function of *Itgb3* in CA3 pyramidal neurons before or after postnatal day 30. Although we carefully considered data clustering, it was not possible to conclude if other factors besides genotype affected the dendritic morphology studied here. We cannot eliminate the possibility that there are additional nonlinear relationships between pairs of topographic and/or morphological variables in either WT or cKO neurons. Finally, we did not test the haploinsufficiency of *Itgb3* by including conditional or full heterozygotes, which have been reported in behavioral studies (Lopuch et al., 2022; Mazaloukas et al., 2015).

Together with its role in regulating dendritic structure in the cerebral cortex, we conclude that integrin $\beta 3$ has a critical function *in vivo* for regulating dendritic morphology of CA3 pyramidal neurons in the hippocampus.

ACKNOWLEDGMENTS

We wish to acknowledge the excellent animal care provided by Mses. Stephanie Atkins and Sarah Keegan.

FUNDING INFORMATION

Funding was provided by the National Institute of Neurological Disorders and Stroke (K01NS107723).

CONFLICT OF INTEREST STATEMENT

The authors have no conflict of interest to declare.

DATA AVAILABILITY STATEMENT

The reconstruction data that support the findings of this study will be made openly available at NeuroMorpho.org (Akram, Nanda, Maraver, Armañanzas, & Ascoli, 2018; Ascoli, Donohue, & Halavi, 2007). Other data are available from the corresponding author upon reasonable request.

ORCID

George S. Vidal  <https://orcid.org/0000-0002-8623-7476>

REFERENCES

- Akram, M. A., Nanda, S., Maraver, P., Armañanzas, R., & Ascoli, G. A. (2018). An open repository for single-cell reconstructions of the brain forest. *Scientific Data*, 5, 180006. <https://doi.org/10.1038/sdata.2018.6>
- Ascoli, G. A., Donohue, D. E., & Halavi, M. (2007). NeuroMorpho.Org: A central resource for neuronal morphologies. *The Journal of Neuroscience*, 27(35), 9247–9251. <https://doi.org/10.1523/JNEUROSCI.2055-07.2007>

- Barón-Mendoza, I., Del Moral-Sánchez, I., Martínez-Marcial, M., García, O., Garzón-Cortés, D., & González-Arenas, A. (2019). Dendritic complexity in prefrontal cortex and hippocampus of the autistic-like mice C58/J. *Neuroscience Letters*, 703, 149–155. <https://doi.org/10.1016/j.neulet.2019.03.018>
- Benjamini, Y., Krieger, A. M., & Yekutieli, D. (2006). Adaptive linear step-up procedures that control the false discovery rate. *Biometrika*, 93(3), 491–507. <https://doi.org/10.1093/biomet/93.3.491>
- Carter, M. D., Shah, C. R., Muller, C. L., Crawley, J. N., Carneiro, A. M. D., & Veenstra-VanderWeele, J. (2011). Absence of preference for social novelty and increased grooming in integrin $\beta 3$ knockout mice: Initial studies and future directions. *Autism Research*, 4(1), 57–67. <https://doi.org/10.1002/aur.180>
- Cembrowski, M. S., & Spruston, N. (2019). Heterogeneity within classical cell types is the rule: Lessons from hippocampal pyramidal neurons. *Nature Reviews Neuroscience*, 20(4), 193–204. <https://doi.org/10.1038/s41583-019-0125-5>
- Chan, C.-S., Weeber, E. J., Kurup, S., Sweatt, J. D., & Davis, R. L. (2003). Integrin requirement for hippocampal synaptic plasticity and spatial memory. *The Journal of Neuroscience*, 23(18), 7107–7116. <https://doi.org/10.1523/JNEUROSCI.23-18-07107.2003>
- Chavis, P., & Westbrook, G. (2001). Integrins mediate functional pre- and postsynaptic maturation at a hippocampal synapse. *Nature*, 411(6835), 317–321. <https://doi.org/10.1038/35077101>
- Cingolani, L. A., & Goda, Y. (2008). Differential involvement of beta3 integrin in pre- and postsynaptic forms of adaptation to chronic activity deprivation. *Neuron Glia Biology*, 4(3), 179–187. <https://doi.org/10.1017/S1740925X0999024X>
- Cingolani, L. A., Thalhammer, A., Yu, L. M. Y., Catalano, M., Ramos, T., Colicos, M. A., & Goda, Y. (2008). Activity-dependent regulation of synaptic AMPA receptor composition and abundance by $\beta 3$ integrins. *Neuron*, 58(5), 749–762. <https://doi.org/10.1016/j.neuron.2008.04.011>
- Cloarec, R., Riffault, B., Dufour, A., Rabiei, H., Gouty-Colomer, L.-A., Dumon, C., Guimond, D., Bonifazi, P., Eftekhari, S., Lozovaya, N., Ferrari, D. C., & Ben-Ari, Y. (2019). Pyramidal neuron growth and increased hippocampal volume during labor and birth in autism. *Science Advances*, 5(1), eaav0394. <https://doi.org/10.1126/sciadv.aav0394>
- Ding, L., Chen, H., Diamantaki, M., Coletta, S., Preston-Ferrer, P., & Burgalossi, A. (2020). Structural correlates of CA2 and CA3 pyramidal cell activity in freely-moving mice. *The Journal of Neuroscience*, 40(30), 5797–5806. <https://doi.org/10.1523/JNEUROSCI.0099-20.2020>
- Ellegood, J., Henkelman, R. M., & Lerch, J. P. (2012). Neuroanatomical assessment of the integrin $\beta 3$ mouse model related to autism and the serotonin system using high resolution MRI. *Frontiers in Psychiatry*, 3, 37. <https://doi.org/10.3389/fpsy.2012.00037>
- Feng, G., Mellor, R. H., Bernstein, M., Keller-Peck, C., Nguyen, Q. T., Wallace, M., Nerbonne, J. M., Lichtman, J. W., & Sanes, J. R. (2000). Imaging neuronal subsets in transgenic mice expressing multiple spectral variants of GFP. *Neuron*, 28(1), 41–51. [https://doi.org/10.1016/S0896-6273\(00\)00084-2](https://doi.org/10.1016/S0896-6273(00)00084-2)
- Feng, L., Zhao, T., & Kim, J. (2015). neuTube 1.0: A new design for efficient neuron reconstruction software based on the SWC format. *ENeuro*, 2(1), ENEURO.0049-ENEU14.2014. <https://doi.org/10.1523/ENeuro.0049-14.2014>
- Ferreira, T. A., Blackman, A. V., Oyrer, J., Jayabal, S., Chung, A. J., Watt, A. J., Sjöström, P. J., & van Meyel, D. J. (2014). Neuronal morphometry directly from bitmap images. *Nature Methods*, 11(10), 982–984. <https://doi.org/10.1038/nmeth.3125>
- Gorski, J. A., Talley, T., Qiu, M., Puelles, L., Rubenstein, J. L. R., & Jones, K. R. (2002). Cortical excitatory neurons and glia, but not GABAergic neurons, are produced in the Emx1-expressing lineage. *The Journal of Neuroscience*, 22(15), 6309–6314. <https://doi.org/10.1523/JNEUROSCI.22-15-06309.2002>
- Handwerk, C. J., Bland, K. M., Brett, C. A., Denzler, C. J., Kalinowski, A. R., Swinehart, B. D., & Vidal, G. S. (2022). A cellular positioning system to probe morphological heterogeneity among mouse CA3 hippocampal pyramidal neurons (p. 2022.08.12.503761). p. 2022.08.12.503761. bioRxiv. <https://doi.org/10.1101/2022.08.12.503761>
- Hemond, P., Migliore, M., Ascoli, G. A., & Jaffe, D. B. (2009). The membrane response of hippocampal CA3b pyramidal neurons near rest: Heterogeneity of passive properties and the contribution of hyperpolarization-activated currents. *Neuroscience*, 160(2), 359–370. <https://doi.org/10.1016/j.neuroscience.2009.01.082>
- Hemond, P., Epstein, D., Boley, A., Migliore, M., Ascoli, G. A., & Jaffe, D. B. (2008). Distinct classes of pyramidal cells exhibit mutually exclusive firing patterns in hippocampal area CA3b. *Hippocampus*, 18(4), 411–424. <https://doi.org/10.1002/hipo.20404>
- Herrera-Molina, R., Frischknecht, R., Maldonado, H., Seidenbecher, C. I., Gundelfinger, E. D., Hetz, C., Aylwin, M. L., Schneider, P., Quest, A. F. G., & Leyton, L. (2012). Astrocytic $\alpha \beta 3$ integrin inhibits neurite outgrowth and promotes retraction of neuronal processes by clustering Thy-1. *PLoS One*, 7(3), e34295. <https://doi.org/10.1371/journal.pone.0034295>
- Hunt, D. L., Linaro, D., Si, B., Romani, S., & Spruston, N. (2018). A novel pyramidal cell type promotes sharp-wave synchronization in the hippocampus. *Nature Neuroscience*, 21(7), 985–995. <https://doi.org/10.1038/s41593-018-0172-7>
- Ishizuka, N., Cowan, W. M., & Amaral, D. G. (1995). A quantitative analysis of the dendritic organization of pyramidal cells in the rat hippocampus. *The Journal of Comparative Neurology*, 362(1), 17–45. <https://doi.org/10.1002/cne.903620103>
- Jaudon, F., Thalhammer, A., & Cingolani, L. A. (2021). Integrin adhesion in brain assembly: From molecular structure to neuropsychiatric disorders. *The European Journal of Neuroscience*, 53(12), 3831–3850. <https://doi.org/10.1111/ejn.14859>
- Kang, W.-S., Choi, J.-S., Shin, Y.-J., Kim, H.-Y., Cha, J.-H., Lee, J.-Y., Chun, M. H., & Lee, M. Y. (2008). Differential regulation of osteopontin receptors, CD44 and the $\alpha \nu$ and $\beta 3$ integrin subunits, in the rat hippocampus following transient forebrain ischemia. *Brain Research*, 1228, 208–216. <https://doi.org/10.1016/j.brainres.2008.06.106>
- Kerrisk, M. E., Greer, C. A., & Koleske, A. J. (2013). Integrin $\alpha 3$ is required for late postnatal stability of dendrite arbors, dendritic spines and synapses, and mouse behavior. *The Journal of Neuroscience*, 33(16), 6742–6752. <https://doi.org/10.1523/JNEUROSCI.0528-13.2013>
- Kesner, R. P. (2007). Behavioral functions of the CA3 subregion of the hippocampus. *Learning & Memory*, 14(11), 771–781. <https://doi.org/10.1101/lm.688207>
- Krichmar, J. L., Nasuto, S. J., Scorcioni, R., Washington, S. D., & Ascoli, G. A. (2002). Effects of dendritic morphology on CA3 pyramidal cell electrophysiology: A simulation study. *Brain Research*, 941(1), 11–28. [https://doi.org/10.1016/S0006-8993\(02\)02488-5](https://doi.org/10.1016/S0006-8993(02)02488-5)
- Li, X.-G., Somogyi, P., Ylinen, A., & Buzsáki, G. (1994). The hippocampal CA3 network: An in vivo intracellular labeling study. *Journal of Comparative Neurology*, 339(2), 181–208. <https://doi.org/10.1002/cne.903390204>
- Lilja, J., & Ivaska, J. (2018). Integrin activity in neuronal connectivity. *Journal of Cell Science*, 131(12), jcs212803. <https://doi.org/10.1242/jcs.212803>
- Longair, M. H., Baker, D. A., & Armstrong, J. D. (2011). Simple neurite tracer: Open source software for reconstruction, visualization and analysis of neuronal processes. *Bioinformatics (Oxford, England)*, 27(17), 2453–2454. <https://doi.org/10.1093/bioinformatics/btr390>
- Lopuch, A. J., Swinehart, B. D., Widener, E. L., Holley, Z. L., Bland, K. M., Handwerk, C. J., Brett, C. A., Cook, H. N., Kalinowski, A. R., Rodriguez, H. V., Song, M. L., & Vidal, G. S. (2022). Integrin $\beta 3$ in forebrain Emx1-expressing cells regulates repetitive self-grooming and sociability in mice. *BMC Neuroscience*, 23(1), 12–16. <https://doi.org/10.1186/s12868-022-00691-2>

- Malik, R., Dougherty, K. A., Parikh, K., Byrne, C., & Johnston, D. (2016). Mapping the electrophysiological and morphological properties of CA1 pyramidal NEURONS along the longitudinal hippocampal axis: DORSOVENTRAL GRADIENT IN EXCITABILITY OF CA1 NEURONS. *Hippocampus*, 26(3), 341–361. <https://doi.org/10.1002/hipo.22526>
- Mazaloukas, M., Jessen, T., Varney, S., Sutcliffe, J. S., Veenstra-VanderWeele, J., Cook, E. H., & Carneiro, A. M. D. (2015). Integrin β 3 haploinsufficiency modulates serotonin transport and antidepressant-sensitive behavior in mice. *Neuropsychopharmacology*, 40(8), 2015–2024. <https://doi.org/10.1038/npp.2015.51>
- McGeachie, A. B., Skrzypiec, A. E., Cingolani, L. A., Letellier, M., Pawlak, R., & Goda, Y. (2012). B3 integrin is dispensable for conditioned fear and hebbian forms of plasticity in the hippocampus. *The European Journal of Neuroscience*, 36(4), 2461–2469. <https://doi.org/10.1111/j.1460-9568.2012.08163.x>
- Morgan, E. A., Schneider, J. G., Baroni, T. E., Uluçkan, O., Heller, E., Hurchla, M. A., Deng, H., Floyd, D., Berdy, A., Prior, J. L., Piwnicka-Worms, D., L. Teitelbaum, S., Patrick Ross, F., & Weilbaecher, K. N. (2010). Dissection of platelet and myeloid cell defects by conditional targeting of the beta3-integrin subunit. *FASEB Journal*, 24(4), 1117–1127. <https://doi.org/10.1096/fj.09-138420>
- Park, Y. K., & Goda, Y. (2016). Integrins in synapse regulation. *Nature Reviews Neuroscience*, 17(12), 745–756. <https://doi.org/10.1038/nrn.2016.138>
- Perez-Rosello, T., Baker, J. L., Ferrante, M., Iyengar, S., Ascoli, G. A., & Barrionuevo, G. (2011). Passive and active shaping of unitary responses from associational/commissural and perforant path synapses in hippocampal CA3 pyramidal cells. *Journal of Computational Neuroscience*, 31(2), 159–182. <https://doi.org/10.1007/s10827-010-0303-y>
- Pozo, K., Cingolani, L. A., Bassani, S., Laurent, F., Passafaro, M., & Goda, Y. (2012). B3 integrin interacts directly with GluA2 AMPA receptor subunit and regulates AMPA receptor expression in hippocampal neurons. *Proceedings of the National Academy of Sciences*, 109(4), 1323–1328. <https://doi.org/10.1073/pnas.1113736109>
- Riccardi, S., Cingolani, L. A., & Jaudon, F. (2022). CRISPR-mediated activation of α V integrin subtypes promotes neuronal differentiation of neuroblastoma Neuro2a cells. *Frontiers in Genome Editing*, 4, 1–12. <https://www.frontiersin.org/articles/10.3389/fgeed.2022.846669>
- Schindelin, J., Arganda-Carreras, I., Frise, E., Kaynig, V., Longair, M., Pietzsch, T., Preibisch, S., Rueden, C., Saalfeld, S., Schmid, B., Tinevez, J. Y., White, D. J., Hartenstein, V., Eliceiri, K., Tomancak, P., & Cardona, A. (2012). Fiji: An open-source platform for biological-image analysis. *Nature Methods*, 9(7), 676–682. <https://doi.org/10.1038/nmeth.2019>
- Scorcioni, R., Polavaram, S., & Ascoli, G. A. (2008). L-measure: A web-accessible tool for the analysis, comparison and search of digital reconstructions of neuronal morphologies. *Nature Protocols*, 3(5), 866–876. <https://doi.org/10.1038/nprot.2008.51>
- Shi, Y., & Ethell, I. M. (2006). Integrins control dendritic spine plasticity in hippocampal neurons through NMDA receptor and Ca²⁺/calmodulin-dependent protein kinase II-mediated Actin reorganization. *The Journal of Neuroscience*, 26(6), 1813–1822. <https://doi.org/10.1523/JNEUROSCI.4091-05.2006>
- Sholl, D. A. (1953). Dendritic organization in the neurons of the visual and motor cortices of the cat. *Journal of Anatomy*, 87(Pt 4), 387–406.1.
- Sun, Q., Jiang, Y.-Q., & Lu, M. C. (2020). Topographic heterogeneity of intrinsic excitability in mouse hippocampal CA3 pyramidal neurons. *Journal of Neurophysiology*, 124(4), 1270–1284. <https://doi.org/10.1152/jn.00147.2020>
- Sun, Q., Sotayo, A., Cazzulino, A. S., Snyder, A. M., Denny, C. A., & Siegelbaum, S. A. (2017). Proximodistal heterogeneity of hippocampal CA3 pyramidal neuron intrinsic properties, connectivity, and reactivation during memory recall. *Neuron*, 95(3), 656–672.e3. <https://doi.org/10.1016/j.neuron.2017.07.012>
- Swinehart, B. D., Bland, K. M., Holley, Z. L., Lopuch, A. J., Casey, Z. O., Handwerk, C. J., & Vidal, G. S. (2020). Integrin β 3 organizes dendritic complexity of cerebral cortical pyramidal neurons along a tangential gradient. *Molecular Brain*, 13(1), 1–15. <https://doi.org/10.1186/s13041-020-00707-0>
- Turner, D. A., Li, X.-G., Pyapali, G. K., Ylinen, A., & Buzsaki, G. (1995). Morphometric and electrical properties of reconstructed hippocampal CA3 neurons recorded in vivo. *Journal of Comparative Neurology*, 356(4), 580–594. <https://doi.org/10.1002/cne.903560408>
- Varney, S., Polston, K. F., Jessen, T., & Carneiro, A. M. D. (2015). Mice lacking integrin β 3 expression exhibit altered response to chronic stress. *Neurobiology of Stress*, 2, 51–58. <https://doi.org/10.1016/j.ynstr.2015.05.002>
- Warren, M. S., Bradley, W. D., Gourley, S. L., Lin, Y.-C., Simpson, M. A., Reichardt, L. F., Greer, C. A., Taylor, J. R., & Koleske, A. J. (2012). Integrin β 1 signals through Arg to regulate postnatal dendritic arborization, synapse density, and behavior. *The Journal of Neuroscience*, 32(8), 2824–2834. <https://doi.org/10.1523/JNEUROSCI.3942-11.2012>
- Wilson, M. D., Sethi, S., Lein, P. J., & Keil, K. P. (2017). Valid statistical approaches for analyzing sholl data: Mixed effects versus simple linear models. *Journal of Neuroscience Methods*, 279, 33–43. <https://doi.org/10.1016/j.jneumeth.2017.01.003>
- Witter, M. P. (2007). Intrinsic and extrinsic wiring of CA3: Indications for connectional heterogeneity. *Learning & Memory*, 14(11), 705–713. <https://doi.org/10.1101/lm.725207>
- Yu, Z., Guindani, M., Grieco, S. F., Chen, L., Holmes, T. C., & Xu, X. (2022). Beyond t test and ANOVA: Applications of mixed-effects models for more rigorous statistical analysis in neuroscience research. *Neuron*, 110(1), 21–35. <https://doi.org/10.1016/j.neuron.2021.10.030>

SUPPORTING INFORMATION

Additional supporting information can be found online in the Supporting Information section at the end of this article.

How to cite this article: Handwerk, C. J., Denzler, C. J., Kalinowski, A. R., Cook, H. N., Rodríguez, H. V., Bland, K. M., Brett, C. A., Swinehart, B. D., Vinson, E. C., & Vidal, G. S. (2023). Integrin β 3 regulates apical dendritic morphology of pyramidal neurons throughout hippocampal CA3. *Hippocampus*, 33(8), 936–947. <https://doi.org/10.1002/hipo.23530>